Anisotropy of the electron momentum distribution in α-quartz investigated by Compton scattering and *ab initio* simulations

Cesare Pisani,[1] Alessandro Erba,[1] Silvia Casassa,[1] Masayoshi Itou,[2] and Yoshiharu Sakurai[2]

[1]*Dipartimento di Chimica IFM and Centre of Excellence NIS (Nanostructured Interfaces and Surfaces), Università di Torino, via P. Giuria 5, I-10125 Torino, Italy*

[2]*Japan Synchrotron Radiation Research Institute (JASRI), 1-1-1 Kouto, Sayo, Hyogo 679-5198, Japan*

The Compton profiles of α-quartz have been measured along 30 crystallographically independent directions with an experimental resolution of 0.11 atomic units in full width at half maximum. They are critically compared to those obtained from periodic quantum-chemical simulations based on the use of density-functional, Hartree-Fock, and post-Hartree-Fock approximations. The anisotropy of the electron momentum distribution, which clearly emerges from both the experiment and the theory, is analyzed and explained in terms of contributions from the localized Wannier functions associated with the Si–O bonds and with the lone pairs on the oxygen atoms.

I. INTRODUCTION

Based on the early work of Coulson,[1,2] much attention has been given in past years to the electron momentum distribution (EMD) of chemical systems (molecules, crystals). Although not uniquely,[3] the EMD [$\pi(\mathbf{p})$] can be reconstructed from the outcome of Compton scattering experiments and can provide valuable information on the electronic structure of the system, complementary to that embodied in the electron charge distribution (ECD) $\rho(\mathbf{r})$ as obtainable from diffraction measurements. Many studies have been performed, mainly theoretical in character, aimed at finding correlations between the EMD features and the chemical characteristics of the system: see, for example, Refs. 4–10. Parallel work went on concerning the analysis of the results from binary (e,$2e$) spectroscopy, which provides more subtle information on the momentum density of individual molecular orbitals,[11,12] but we are not concerned with this topic here.

The analysis performed in those studies was generally based on a partition of the EMD among contributions from substructures of the system, starting from knowledge of the ground-state wave function. Cooper and Allan,[8] for instance, used a valence-bond approach to individualize the spin-coupled orbital responsible for the bond formation of three simple diatomic molecules (BH^+, LiH, and LiH^+) and analyzed its evolution in momentum space as a function of the internuclear distance. Only rarely is the Schrödinger equation solved directly in momentum space (where it becomes an integral equation); most commonly, it is solved in position space and then the wave function is Fourier transformed. Localization techniques in position space[13] have been used for partitioning the total EMD into chemically significant contributions from bonds, lone pairs, etc.[4] It turned out that simple guidelines for the analysis of the EMD were not generally applicable. For instance, the *bond-directional principle* tentatively formulated by Epstein and Tanner,[5] according to which "the momentum of an electron in a chemical bond is more likely to be directed perpendicular to than along the bond axis," was disproved in many cases.[9] As a matter of fact, the contribution of a pair of electrons in a chemical bond to the EMD was found to depend not only on the quality of the wave function and

on the scheme of localization adopted, but also, and even primarily, on the kind of atomic orbitals involved in the bond, which may result in quite complex structures.[7] The possibility of identifying such chemically significant components of the total EMD is tantalizing, but it is generally frustrated by a sort of *compensation principle* that seems to be generally valid: "the total EMD of a many-electron system is much closer to its spherical average than the individual contributions from chemically significant substructures"; in other words, anisotropies in momentum space coming from a substructure are likely to be largely compensated by those from the other substructures.

The question can then be asked whether it is sensible and worthwhile to analyze the total EMD in terms of separate contributions. Our answer is (cautiously) in the affirmative for two main reasons. First, some trace of the individual anisotropies must be left that is hopefully transferable, approximately at least, to systems containing the same chemical ingredient. Second, it is easier and more informative to recognize the effect of the level of theory employed (basis set, Hamiltonian, etc.) on the description in momentum space of specific substructures. A special but important issue in this respect is the influence of instantaneous Coulomb correlation on the EMD. It has been recently argued that this effect, not explicitly embodied in mean-field Hamiltonians like those of Hartree-Fock (HF) or density-functional theory (DFT), can play a non-negligible role; in the cases of urea[14] and silicon,[15,16] its consideration has been shown to bring the calculated EMD into closer agreement with the experiment.

Testing the feasibility and usefulness of such an analysis through a comparison between experiment and theory requires the fulfillment of some conditions: (i) a set of crystalline systems should be considered which share similar chemical substructures that are differently arranged; (ii) for a few of them, very good experimental determinations of the EMD should be available, revealing appreciable anisotropies; (iii) an accurate theoretical evaluation of their density matrices (DMs) should be feasible; (iv) a "universal" and "transferable" partition of the theoretical EMD into local contributions should be used.

This work is a first step in this direction. It concerns the EMD properties of α-quartz, the prototype of silica polymorphs $[(SiO_2)_n]$, a class of systems comprising an astounding variety of crystalline structures, all characterized by silicon surrounded by oxygen atoms in a tetrahedral coordination. Its crystalline structure is simple yet nontrivial. It belongs to the trigonal system (space group $P3_221$) and comprises just three SiO_2 units in the primitive cell, equivalent by symmetry but differently oriented. In principle, comparison of its EMD with that of a few simple compounds of the same family could meet the first of the requirements just listed.

The situation is less encouraging as concerns the second condition. To our knowledge, only two previous determinations are available of the EMD properties of α-quartz through Compton profile (CP) experiments. Rosenberg *et al.*[17] used 159-keV γ rays to compare the inelastic scattering properties of amorphous and single-crystal quartz. They found that the anisotropy in the latter case was only slightly above the detectability threshold (their resolution in momentum space was 0.202 a.u.), about an order of magnitude smaller than observed in typical covalent systems like silicon. By means of theoretical simulations, they were able to reproduce the experimental data to within 1% using a purely ionic $(Si^{4+} + O^{2-})$ model. The lack of appreciable bond charges combined with the different orientations of the various ion-ion pairs was suggested as a possible explanation for the absence of measurable EMD anisotropy. A few years later Mahapatra and Padhi[18] confirmed those findings. They also provided a different proof of the ionic character of α-quartz, using a naive scaling principle to compare its average CP with that of other typical ionic crystals. The advances in CP techniques in the last 30 years allow us presently to collect data of unprecedented accuracy. At the High Energy Inelastic (BL08W) beamline of SPring-8, a rich set of directional CPs of α-quartz have been measured, as described in detail in Sec. II, which carry definite evidence of EMD anisotropy.

Similar progress has taken place in the *ab initio* simulation of crystalline systems. We are using here two well-documented computer programs. CRYSTAL (Refs. 19 and 20) solves the periodic Schrödinger equation in a one-electron (HF, DFT, or hybrid-exchange) approximation and determines from there a variety of crystalline properties, related either to the energy or to the DM. CRYSCOR (Refs. 21–25) starts from the HF solution provided by CRYSTAL and corrects it using many-body perturbation theory truncated at second order (the so-called Møller-Plesset-2 or MP2 approximation); we are here mainly interested in the effect of such a post-HF correction on the EMD. Both programs adopt a basis set of local, atomiclike functions, the Gaussian-type orbitals (GTOs), which needs careful calibration. Details of the computational setup are provided in Sec. III.

Consider now the last requirement in the list above. Among the possibilities previously mentioned for the partition of the DM into local contributions, the use of Wannier functions[26,27] (WFs) appears particularly suitable for periodic, nonconducting systems described by one-electron Hamiltonians, and it is the one here adopted. WFs are real-valued, well-localized functions of **r** which span altogether the same functional space as the occupied crystalline orbitals and are translationally

equivalent to each other and mutually orthonormal. Symmetry-adapted WFs (Ref. 28) are generated by CRYSTAL after solution of the one-electron problem and are an essential ingredient for the post-HF technique adopted in CRYSCOR, which is based on a local-correlation scheme first proposed by Pulay.[29] This kind of partition, although not unique, presents some attractive features. First, WFs are generated following a nonarbitrary prescription;[28] it has recently been shown that the scheme adopted for the symmetrization maximizes in most cases the equivalences among the WFs.[30] Second, they usually can be identified with definite chemical substructures of the system. Third, and precisely for the above reason, their essential features are retained in chemically similar crystals. It is shown below that the partition of the DM into WF contributions still makes sense when post-HF corrections are taken into account, but requires some care.

The present experimental EMD data are compared to the simulated ones in Sec. IV. The measured CPs reveal an anisotropy of the EMD which, though small, is clearly larger than the experimental error. They are closely reproduced by the calculated profiles, the agreement being better with the HF and (especially) the post-HF data. The analysis of the contribution to the EMD from the various WFs allows us to relate the observed anisotropy to the bonding structure of the crystal.

II. THE EXPERIMENT

We have collected two sets of directional CPs of α-quartz at the BL08W beamline of SPring-8 in Japan: 19 CPs $J(p;\theta)$ in the vertical plane and 11 CPs $J(p;\phi)$ in the horizontal plane; the crystallographic direction is here represented by the two angles θ and ϕ instead of Miller's indices $[hkl]$. θ spans the vertical plane from the [001] ($\theta = 0°$) to the [210] ($\theta = 90°$) direction; ϕ spans the horizontal plane from the [100] ($\phi = 0°$) to the [210] ($\phi = 30°$) direction. See Sec. IV B for a graphical definition of such angles. Single crystals of α-quartz with a cylindrical shape of 5 mm in diameter and 5 mm in height were used. The direction normal to the circular plane is [010] or [001] so that a set of $J(p;\theta)$ or $J(p;\phi)$ profiles has been measured by keeping the same geometrical shape of the samples for all directions. This leads to almost perfect cancellation of multiple-scattering contributions in the CP anisotropies. The experiment was carried out at room temperature. The incident x-ray energy was 115.56 keV and the photon flux at the sample is 1×10^{13} photons/s. The energy profiles of Compton-scattered x rays were measured at the scattering angle of 163.8° using the Cauchois-type high-resolution Compton-scattering spectrometer.[31,32] The overall instrumental resolution was 0.11 a.u. in full width at half maximum. The measured profiles were corrected for absorption, detection efficiency, scattering cross section, and multiple-scattering contributions. Areas under the corrected profiles were normalized to the total number of electrons, and the normalized profiles were used as total CPs. For the multiple-scattering correction, we used the profile of silicon determined by a separate experiment and evaluated the intensity of multiple scattering by a Monte Carlo simulation.[33] The valence CPs were obtained by subtracting from the total the core-electron contribution.[34]

III. THE THEORETICAL PROCEDURE

A. Partitioning the EMD into WF contributions

As mentioned in the Introduction, WFs are translationally equivalent and mutually orthonormal functions of $\mathbf{r}$:

$$W_{i,\mathbf{0}}(\mathbf{r}) = W_{i,\mathbf{g}}(\mathbf{r} + \mathbf{g}), \tag{1}$$

$$\int W_{i,\mathbf{g}}(\mathbf{r}) W_{i',\mathbf{g}'}(\mathbf{r}) d\mathbf{r} = \delta_{ii'} \delta_{\mathbf{gg}'}. \tag{2}$$

Here, $\mathbf{g}$ and $\mathbf{g}'$ are lattice vectors of the L-cyclic crystal with Born von Kármán periodic boundary conditions. WFs span altogether the same functional space as the occupied canonical crystalline orbitals (COs) $\psi_{j,\kappa}(\mathbf{r})$, the label κ identifying one of the L-allowed $\mathbf{k}$ points in the first Brillouin zone of the reciprocal space, while j is the band index which runs from 1 to $N_0/2$ for closed-shell crystals, N_0 being the number of electrons per cell. We are interested here only in *valence* WFs, which provide the anisotropic part of the EMD, and span the space defined by the $N_v/2$ occupied COs highest in energy, N_v being the number of valence electrons per cell (24 in the present case). In CRYSTAL, COs are expressed as a linear combination of atomic orbitals (AOs), with coefficients depending on the Hamiltonian adopted [X indicates the HF, local-density approximation (LDA), Perdew-Burke-Ernzerhof (PBE), or Becke three-parameter Lee-Yang-Parr (B3LYP) Hamiltonian; in the following, the superscript X is omitted when not needed]:

$$\hat{h}^X \psi_{j,\kappa}^X(\mathbf{r}) = \varepsilon_{j,\kappa}^X \, \psi_{j,\kappa}^X(\mathbf{r}), \tag{3}$$

$$\psi_{j,\kappa}^X(\mathbf{r}) = \sum_\mu a_{j,\kappa;\mu}^X \left[\sum_{\mathbf{g}} e^{\iota \kappa \cdot \mathbf{g}} \chi_\mu^{\mathbf{g}}(\mathbf{r} - \mathbf{r}_\mu) \right]. \tag{4}$$

As is standard practice in molecular quantum chemistry, the AOs are contractions of GTOs of angular momentum components (ℓ, m), generally centered in an atomic nucleus:

$$\chi_\mu^{\mathbf{g}}(\mathbf{r} - \mathbf{r}_\mu) = \sum_{h=1}^{M_\mu} c_{\mu,h} G^{\ell,m}(\mathbf{r} - \mathbf{r}_\mu - \mathbf{g}; \alpha_{\mu,h}),$$

$$\tag{5}$$

$$G^{\ell,m}(\mathbf{r}; \alpha) = N^{\ell,m}(\alpha) \left(\sum_{\mathbf{t}}^{(\ell)} D_{\mathbf{t}}^{\ell,m} \prod_{i=1}^{3} x_i^{t_i} \right) \exp[-\alpha r^2].$$

Each "shell" of $2\ell + 1$ AOs is then characterized by its center $\mathbf{r}_\mu$ in the reference zero cell, its "type" ($\ell = s, p, d, f, \ldots$), the number M_μ of GTOs, their "exponent" $\alpha_{\mu,h}$, and their coefficient in the combination $c_{\mu,h}$ ($h = 1, M_\mu$). The general GTO [$G^{\ell,m}(\mathbf{r}; \alpha)$] is a real normalized solid harmonics [$N^{\ell,m}(\alpha)$ is the normalization factor] and is the product of a homogeneous polynomial of degree ℓ in the Cartesian components of $\mathbf{r}$ with a Gaussian function with α exponent centered at the origin.[35]

The WFs are obtained from the occupied COs by virtue of an appropriate unitary transformation that imposes spatial localization and can be expressed as a linear combination of AOs:

$$W_{i,\mathbf{0}}(\mathbf{r}) = \sum_\mu \sum_{\mathbf{g}} w_{i,\mu\mathbf{g}} \chi_\mu^{\mathbf{g}}(\mathbf{r} - \mathbf{r}_\mu). \tag{6}$$

The valence *position* [$\gamma^v(\mathbf{r}; \mathbf{r}')$] and *momentum* [$\gamma^v(\mathbf{p}; \mathbf{p}')$] one-electron DMs of a crystalline, nonconducting, closed-shell

system obtained with a one-electron Hamiltonian can be expressed in terms of WFs as follows:

$$\gamma^v(\mathbf{r}; \mathbf{r}') = \frac{2}{L} \sum_i^{N_v/2} \sum_{\mathbf{g}}^{L} W_{i,\mathbf{g}}(\mathbf{r}) W_{i,\mathbf{g}}(\mathbf{r}') \tag{7}$$

$$\updownarrow \text{ 6D FT} \tag{8}$$

$$\gamma^v(\mathbf{p}; \mathbf{p}') = \frac{2}{L} \sum_i^{N_v/2} \sum_{\mathbf{g}}^{L} W_{i,\mathbf{g}}(\mathbf{p}) W_{i,\mathbf{g}}^*(\mathbf{p}'),$$

where $W_{i,\mathbf{g}}(\mathbf{p})$ is the Fourier transform (FT) of $W_{i,\mathbf{g}}(\mathbf{r})$:

$$W_{i,\mathbf{g}}(\mathbf{p}) \equiv \mathcal{F}[W_{i,\mathbf{g}}(\mathbf{r})]$$
$$= e^{-\iota \mathbf{p} \cdot \mathbf{g}} \sum_\mu \sum_{\mathbf{g}'} w_{i;\mu\mathbf{g}'} e^{-\iota \mathbf{p} \cdot (\mathbf{r}_\mu + \mathbf{g}')} \chi_\mu(\mathbf{p}),$$

$$\chi_\mu(\mathbf{p}) = \mathcal{F}[\chi_\mu^{\mathbf{0}}(\mathbf{r})] = \sum_{h=1}^{M_\mu} c_{\mu,h} \mathcal{F}[G^{\ell,m}(\mathbf{r}; \alpha_{\mu,h})]. \tag{9}$$

The FT of GTOs that appears in the last line can be given a closed analytical expression.[36]

The diagonal parts of the one-electron DMs of Eqs. (7) and (8) are the ECD $\rho(\mathbf{r}) \equiv \gamma(\mathbf{r}; \mathbf{r})$ and the EMD $\pi(\mathbf{p}) \equiv \gamma(\mathbf{p}; \mathbf{p})$. It is worth noting that a direct transformation between ECD and EMD is not possible. Precisely due to this missing link, DFT, which is explicitly calibrated on the ECD, is not expected to provide a satisfactory description of the EMD and related quantities.[14–16,37–40]

A convenient expression of the valence EMD is then obtained:

$$\pi^v(\mathbf{p}) = \frac{2}{L} \sum_i^{N_v/2} \sum_{\mathbf{g}}^{L} W_{i,\mathbf{g}}(\mathbf{p}) W_{i,\mathbf{g}}^*(\mathbf{p})$$

$$= 2 \sum_{i=1}^{N_v/2} |W_{i,\mathbf{0}}(\mathbf{p})|^2 = \sum_{i=1}^{N_v/2} \pi_i(\mathbf{p}). \tag{10}$$

In the second passage we have exploited the translational equivalence of the WFs property (1) and in the last one we have partitioned the total EMD $\pi(\mathbf{p})$ into contributions $\pi_i(\mathbf{p})$ from the different WFs:

$$\pi_i(\mathbf{p}) = 2 \sum_{\mu\nu} \sum_{\mathbf{gg}'} w_{i;\mu\mathbf{g}} w_{i;\nu\mathbf{g}'} e^{-\iota \mathbf{p} \cdot (\mathbf{r}_\mu - \mathbf{r}_\nu + \mathbf{g} - \mathbf{g}')} \chi_\mu(\mathbf{p}) \chi_\nu^*(\mathbf{p}).$$

$$\tag{11}$$

The above analysis refers to a single-determinantal solution. It can be interesting, however, to partition in a similar way the *correlation correction* to the EMD. With reference to an AO basis set, the DM either in position ($\mathbf{t}, \mathbf{t}' = \mathbf{r}, \mathbf{r}'$) or in momentum ($\mathbf{t}, \mathbf{t}' = \mathbf{p}, \mathbf{p}'$) space can always be written as follows:

$$\gamma(\mathbf{t}; \mathbf{t}') = \sum_{\mu\nu} \left(P_{\mu\nu}^0 + P_{\mu\nu}' \right) \chi_\mu(\mathbf{t}) \chi_\nu^*(\mathbf{t}'). \tag{12}$$

Here the two P matrices correspond to a "zero" determination of the DM and to its correction at a higher level of approximation, respectively; the labels specifying the center of the AO have been omitted for simplicity. With reference to the HF P^0 matrix, CRYSCOR provides a correcting P' matrix

evaluated in the MP2 approximation following a Lagrangian approach, but without accounting for orbital relaxation.[14,41] On the other hand, the AOs can be expressed in terms of the WFs (defined at the HF level), and of the complementary set of "local orthonormalized orbitals" (LONs) ξ_a which span locally the virtual HF space:[23]

$$\chi_\mu(\mathbf{t}) = \sum_i c_{\mu,i} W_i(\mathbf{t}) + \sum_a d_{\mu,a} \xi_a(\mathbf{t}), \quad (13)$$

$$\text{where} \quad c_{\mu,i} = \langle \mu | i \rangle, \quad d_{\mu,a} = \langle \mu | a \rangle. \quad (14)$$

After substitution in Eq. (12), we can obtain in particular the expression for the correction to the EMD in terms of WFs and LONs:

$$\pi'(\mathbf{p}) = \sum_{ij} A_{ij} W_i(\mathbf{p}) W_j^*(\mathbf{p}) + \sum_{ab} C_{ab} \xi_a(\mathbf{p}) \xi_b^*(\mathbf{p})$$

$$+ \sum_{ia} B_{ia}[W_i(\mathbf{p})\xi_a^*(\mathbf{p}) + W_i^*(\mathbf{p})\xi_a(\mathbf{p})],$$

$$A_{ij} = \sum_{\mu\nu} P'_{\mu\nu} c_{\mu,i} c_{\nu,j}, \quad C_{ab} = \sum_{\mu\nu} P'_{\mu\nu} d_{\mu,a} d_{\nu,b},$$

$$B_{ia} = \sum_{\mu\nu} P'_{\mu\nu} c_{\mu,i} d_{\nu,a}. \quad (15)$$

By use of this expression, the correction to the EMD can be partitioned into WF contributions owing, for instance, to a Mulliken-like procedure, after subdivision of the LONs among the WFs to whose domains they belong.

B. EMD anisotropy and its partition

At variance with the ECD $\rho(\mathbf{r})$, a multicenter periodic function of $\mathbb{R}^3$ which exhibits the whole symmetry of the space group of the system, the EMD $\pi(\mathbf{p})$ is a single-center function of $\mathbb{P}^3$ invariant under the symmetry operations of the point group of the crystal, augmented with the *inversion* arising from the equality $\pi(\mathbf{p}) = \pi(-\mathbf{p})$. Precisely due to its "collapsed" character about the origin $\mathbf{p} = \mathbf{0}$, it is generally difficult to extract the information content of the EMD which is usually revealed in its very subtle features. The partition scheme described above can represent a useful tool for its analysis. A much simpler way of extracting information from the total EMD of a system is by analysis of its anisotropy $\Delta\pi(\mathbf{p})$ with respect to the *spherical average* (SA) function $\pi_{SA}(p)$ which is a "radial" function of a single variable ($p = |\mathbf{p}|$):

$$\Delta\pi(\mathbf{p}) = \pi(\mathbf{p}) - \pi_{SA}(|\mathbf{p}|). \quad (16)$$

According to the proposal of Neutsch,[42] the average value of a function over the surface of a sphere in $\mathbb{P}^3$ can be computed as the average of the function values at the 60 points lying on that surface which form an orbit under the icosahedral group. It can be shown that this definition is exact for all spherical harmonics of degree $\leqslant 9$. Since the EMD is an even function with respect to the inversion of the coordinates, it is sufficient to consider 30 points on the sphere surface. In the present study, we take advantage of the smooth character of $\pi_{SA}(p)$ by explicitly evaluating it on a coarse set of p values and then by interpolating with a cubic spline.

$\Delta\pi(\mathbf{p})$ can be partitioned into contributions from the different valence WFs, since the contribution of core electrons to the anisotropy is negligible:

$$\Delta\pi(\mathbf{p}) = \sum_i^{N_v/2} \Delta\pi_i(\mathbf{p}) \quad \text{with} \quad \Delta\pi_i(\mathbf{p}) = \pi_i(\mathbf{p}) - \frac{\pi_{SA}(p)}{N_v/2}.$$

$$(17)$$

C. Computational settings

Out of the many *ab initio* calculations on α-quartz in the literature, reference is here made to a study recently performed with CRYSTAL,[43] because of the similarity of the techniques with those used here; information on previous work on the subject can be found there. That study was primarily concerned with the effect of the Hamiltonian and basis set on the calculated vibrational spectrum, but also on other properties, in particular the equilibrium geometry. Four one-electron Hamiltonians were there considered which are also used here, namely, HF, a local[44] (LDA) and a generalized-gradient[45] (PBE) formulation of DFT, and a hybrid-exchange scheme (B3LYP).[46] It was shown that, in order to obtain convergence in the calculated properties, a rather sophisticated double-ζ GTO basis set was needed which included two shells of polarization d orbitals per atom. With this basis set excellent agreement between the calculated and the experimental geometry[47] was verified with all Hamiltonians except that in the LDA. This justifies our use of the experimental geometry in all calculations to be described in the following; this choice allows all calculated DMs to be compared to each other and to the experiment. As concerns the vibrational frequencies, B3LYP proved to be the best choice of Hamiltonian, while HF performed definitely worse.

The present basis set corresponds to the best one used in the previous work and includes an f-type shell on both silicon and oxygen. These high-angular-momentum GTOs can play a non-negligible role, especially as concerns the estimate of the correlation corrections.

In CRYSTAL, the truncation of infinite lattice sums is controlled by five thresholds, T1 to T5, which are here set to 15, 15, 15, 25, and 50. The role of T1, here set to the tight value of 15 (instead of 6 which is the default), is of particular relevance for a reliable description of momentum-space properties. The DFT exchange-correlation contribution is evaluated by numerical integration over the cell volume: radial and angular points of the atomic grid are generated through Gauss-Legendre and Lebedev quadrature schemes, using a (75,974)-point grid; grid pruning is adopted. Reciprocal space is sampled with a shrinking factor equal to 15, corresponding to 349 **k** points in the irreducible Brillouin zone.

In CRYSCOR, WFs play an essential role together with the complementary set of projected atomic orbitals (PAOs); the latter are local functions which span the virtual HF manifold.[29] The functions in the two sets will be concisely indicated as $i, j, \ldots$ and $a, b, \ldots$, respectively. As shown in more detail in Sec. IV B, each O in α-quartz has four WFs centered close to it (two lone-pair and two bond WFs), all others being symmetry equivalent. The MP2 energy $E^{(2)}$ can be written as a sum of all contributions E_{ij}^{ab}, each corresponding to

a two-electron excitation from a pair of WFs to a pair of PAOs [$(ij) \uparrow\uparrow (ab)$]; the related amplitudes are calculated via a self-consistent procedure. The input parameters of CRYSCOR serve essentially to fix three kinds of tolerance, all concerning the treatment of WFs and PAOs. The first parameter simply determines the truncation of their tails and is here set to the default value of 10^{-4}. The other two parameters are used to exploit the local-correlation ansatz[29,48] according to which all excitations can be ignored except those involving close-by WF and PAO pairs. With the general WF (i) a domain $\mathcal{D}_i$ is associated consisting of a certain number of atoms close to it; here $\mathcal{D}_i$ is taken to correspond to three atoms (Si–O$^{(i)}$–Si) for lone-pair WFs of O$^{(i)}$ or to six atoms (O$_3$Si$^{(i)}$–O$^{(i)}$–Si) for WFs along the Si$^{(i)}$–O$^{(i)}$ bond. Only those [$(ij) \uparrow\uparrow (ab)$] biexcitations are retained for which both PAOs a and b belong to atoms in $\mathcal{D}_{(i)}$ or $\mathcal{D}_{(j)}$ and the distance d_{ij} between the centers of the two WFs is within a certain value D, here set to 12 Å. Once the relevant WF-PAO pairs are selected, the two-electron repulsion integrals $(ia \mid jb)$ between the respective product distributions are evaluated using a periodic variant of molecular density-fitting techniques,[22,23,25,49] if the two WFs are within a certain distance D', here set to 8 Å; otherwise, a multipolar technique is adopted.

IV. RESULTS AND DISCUSSION

A. Compton profiles: Experiment vs theory

The directional CP $J_{hkl}(p)$ can be obtained through a 2D integration of $\pi(\mathbf{p})$ over a plane perpendicular to $\mathbf{e}_{hkl}$ through $p\,\mathbf{e}_{hkl}$:

$$J_{hkl}(p) = \int \pi(\mathbf{p})\,\delta(\mathbf{p} \cdot \mathbf{e}_{hkl} - p)\,d\mathbf{p}. \tag{18}$$

Due to the linear relation between CPs and EMD, any partition of the latter function results in a partition of the former. The effect of limited experimental resolution characterized by a given standard deviation σ_{CP} (0.047 a.u. in the present case) can be expressed as a convolution of the previous formula with a normalized Gaussian function $g(p; \sigma_{CP})$:

$$J_{hkl}^{\sigma}(p) = \int_{-\infty}^{+\infty} J_{hkl}(p')g(p - p'; \sigma_{CP})\,dp'. \tag{19}$$

Within the sudden-impulse approximation, this function is directly comparable to the outcome of Compton-scattering experiments, after the latter are corrected for multiple-scattering effects as described in Sec. II.

Figure 1 compares the experimental to the simulated CPs along a specific direction, [001]. Since similar results are obtained for the other directions, the considerations that follow are generally valid.

From the upper panel it is seen that the agreement between the experimental and all simulated CPs is very good in the whole range of momentum p here considered, except in the vicinity of the origin ($p < 0.5$ a.u.); at $p = 0$, the theoretical value overestimates the experimental one by about 0.2%. Such disagreement is generally observed.[15] Even if inadequacy of the theoretical simulations cannot be excluded, this discrepancy is more often attributed to an insufficient correction of the experimental data for multiple-scattering effects, and/or to the neglect of nuclear motion effects in the
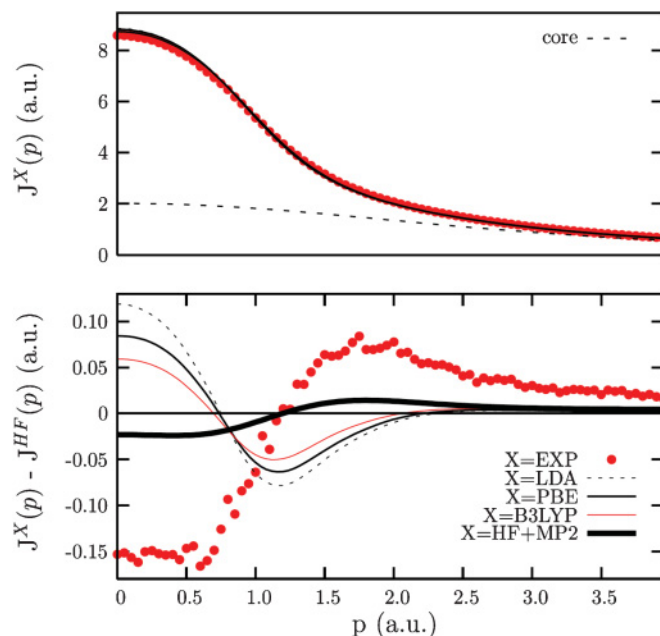

FIG. 1. (Color online) Upper panel: Experimental and simulated total directional CPs along the [001] crystallographic direction. The core contribution to the computed CPs is reported as a dotted line. Lower panel: Difference of the CPs along [001] with respect to the HF one. In both panels, the theoretical CPs are corrected for limited resolution as in Eq. (19).

simulations. As concerns the latter aspect, we recall that all the present calculations refer to static nuclei with the lattice constants set at their experimental value at room temperature. The inclusion of zero-point and thermal motion of the nuclei in the simulation is not an easy task; a detailed study in this direction, including the comparison of experimental versus theoretical CPs of silicon and lithium fluoride at different temperatures, is currently being performed by the present two groups.

More precise information about the influence of the approximation adopted is provided in the lower panel of the same figure, where the HF CP is taken as a reference (note the different vertical scale in the two plots). The following can be noted:

(1) The experimental distribution of electron momenta is displaced to higher values with respect to the HF values, corresponding to a larger expectation value of the kinetic energy T. This is expected: the HF ground-state total energy is known to lie higher than the true one ($E^{HF} > E^0$); due to the virial theorem, which is valid in both cases ($T^{HF} = -E^{HF}$; $T^0 = -E^0$), we must have $T^{HF} < T^0$.

(2) The difference between experiment and theory is reduced after performing the MP2 correction, consistently with the fact that $E^{HF+MP2} < E^{HF}$, but it remains important.

(3) This residual discrepancy can have different explanations: insufficient extent of the correlation correction; experimental errors, especially at low momenta; the fact that the MP2 treatment has been applied only to valence electrons.

(4) For all DFT determinations, the discrepancy with respect to the experiment is in the opposite direction as compared to HF, more so with the LDA than the PBE functional, and
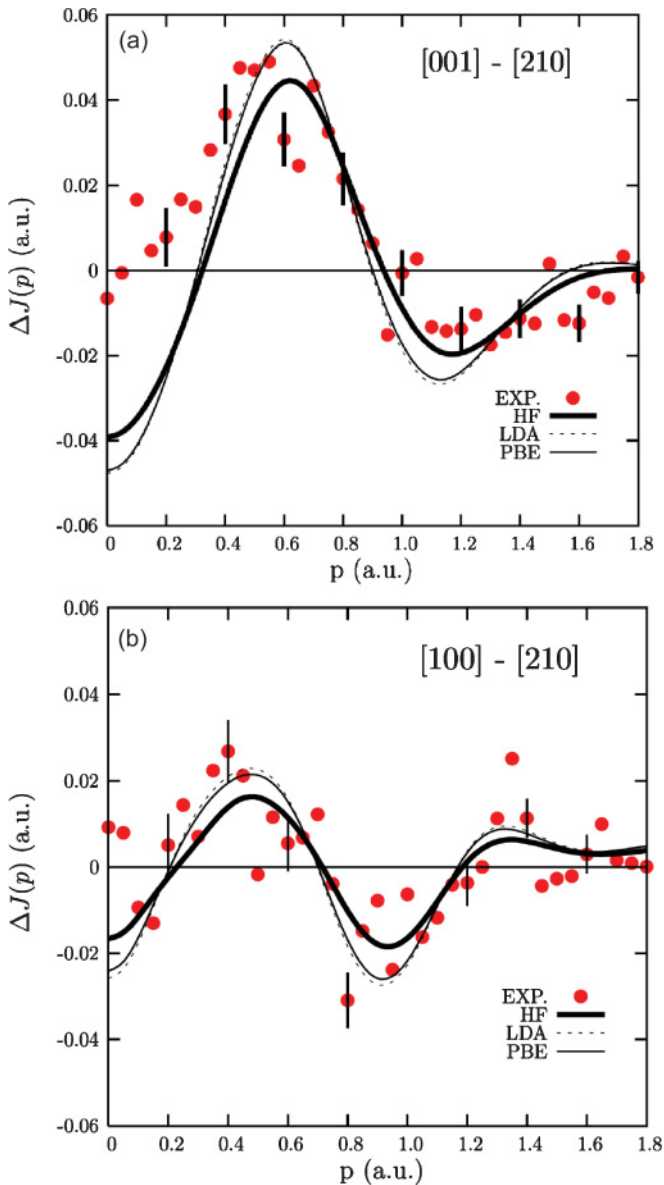
FIG. 2. (Color online) Compton profile anisotropies between different crystallographic directions: (a) [001]-[210] and (b) [100]-[210]. Experimental data (red circles) are compared to the computed data with three different one-electron Hamiltonians: HF (thick black line), LDA (dotted line), and PBE (thin solid line). Some experimental error bars are also reported. The anisotropies are reported in a.u. per SiO_2 formula unit.

less of course with the hybrid B3LYP technique. This fact has been noted also by Thakkar with reference to molecular calculations,[38] and is related to the failure of Kohn-Sham (KS) DFT methods to satisfy the virial theorem, which results generally in their underestimation of the kinetic energy. In the present case, the $-T/E_0$ ratio is 1.0000, 0.9974, 0.9973, and 0.9982, for the HF, LDA, PBE, and B3LYP calculations, respectively.

We report in Fig. 2 the two main CP anisotropies of α-quartz: [001]-[210] and [100]-[210] for the vertical and horizontal planes, respectively. The experimental data with their associated error bars are compared to those simulated

using three one-electron Hamiltonians: HF, LDA, and PBE. We do not report post-HF and B3LYP results at this stage because, from the one hand, MP2 anisotropies are very close to the HF ones and B3LYP data simply lie in between HF and PBE ones. It is seen that (i) the experiment gives clear evidence of the EMD anisotropy in α-quartz, which is however very small as compared, for instance, to that of a fully covalent solid like crystalline silicon,[15] as already noted in previous investigations;[17,18] (ii) the anisotropy is larger (by about a factor of 2) in the vertical than in the horizontal plane; (iii) the noise affecting experimental data does not allow a detailed discussion of the merits and limitations of the different Hamiltonians in reproducing fine features of the EMD; (iv) on the whole, the HF provides closer agreement with the experiment than DFT functionals.

From the data just reported, the known inadequacy of KS DFT as concerns the description of EMD is confirmed. This technique is in fact conceived and calibrated in such a way as to describe a set of independent pseudoparticles which constitute a fictitious noninteracting system and reproduce in principle the *exact* ECD of the ground state of the real system: one cannot expect the same set of occupied KS orbitals to provide its EMD satisfactorily as well.[37,50] From now on, except when indicated, we shall use as a reference the HF determination of the EMD and related quantities.

A more detailed description of the anisotropy of α-quartz in momentum space is provided in Figs. 3 and 4, where we report the whole set of measured CP anisotropies with respect to the average CP $\langle J(p) \rangle = (1/30) \sum_{c=1}^{30} J_c(p)$ as a function of θ and ϕ for the vertical and horizontal planes, respectively. We also report the analogous anisotropies obtained at the HF level for the sake of comparison.

From these data, the larger anisotropy in the vertical with respect to the horizontal plane is confirmed. Inspection of Fig. 3 shows that the experiment definitely reveals the modulation of the anisotropy as a function of θ. For directions close to [001] ($\theta \leqslant 15°$) the anisotropy is large and positive for $p \approx 0.7$ a.u. When $30° \leqslant \theta \leqslant 50°$, the anisotropy is large and positive for $p \approx 1.2$ a.u. and negative for $p \approx 0.7$ a.u.; in the other regions of the vertical plane the anisotropy is smaller and the agreement less satisfactory (see, for instance, the region with $70° \leqslant \theta \leqslant 80°$). The agreement with the simulated data is generally good as concerns both amplitude and position of the oscillations in **p** space.

The same representation is reported in Fig. 4 for the horizontal plane. Here the anisotropies, both measured and calculated, are considerably smaller but still there is good agreement between the two. For directions close to [100] or [210] ($\phi \leqslant 9°$ or $\phi \geqslant 24°$) the anisotropy is slightly more pronounced than in the middle region ($12° \leqslant \phi \leqslant 21°$), where it is almost null.

B. Analysis of the calculated EMD

The statistical noise affecting the present experimental CPs and the fact that they have been sampled only in directions lying in two orthogonal planes does not allow a sufficiently reliable reconstruction of the EMD by well-assessed techniques.[51] The analysis of the EMD and its partition according to the procedures outlined in
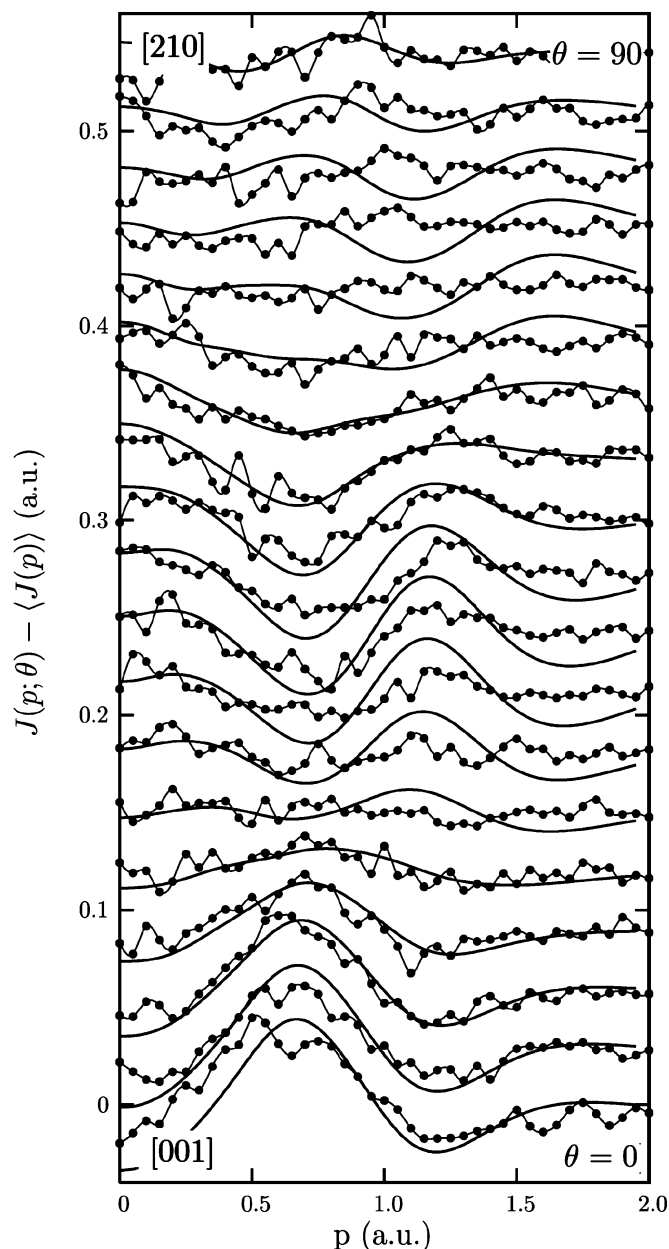
FIG. 3. Anisotropies of the CPs $J(p; \theta)$ with respect to the average CP $\langle J(p) \rangle$ as a function of the angle θ which regularly spans the vertical plane from the [001] direction ($\theta = 0°$) to the [210] direction ($\theta = 90°$). Experimental data are reported as full circles; the theoretical anisotropies (thick continuous lines) are obtained at the HF level. The different anisotropies are upshifted by 0.03 a.u.

FIG. 4. Anisotropies of the CPs $J(p; \phi)$ with respect to the average CP $\langle J(p) \rangle$ as a function of the angle ϕ which regularly spans the horizontal plane from the [100] direction ($\phi = 0°$) to the [210] direction ($\phi = 30°$). The different anisotropies are upshifted by 0.03 a.u. Symbols as in Fig. 3.

Secs. III A and III B will be performed therefore with reference to the HF results.

Figure 5 confirms the picture provided by the CPs, namely, the EMD anisotropy is much larger in the vertical than in the horizontal plane. The region of maximum anisotropy lies at |**p**| values between 1.0 and 1.3 a.u.

Figure 6 provides information about the correlation correction to the EMD along two orthogonal directions, [001] and [210]. As was already apparent from the CPs, its main effect is to increase the velocity of electrons in all directions. At a finer scale, it is seen that the EMD anisotropy estimated at the
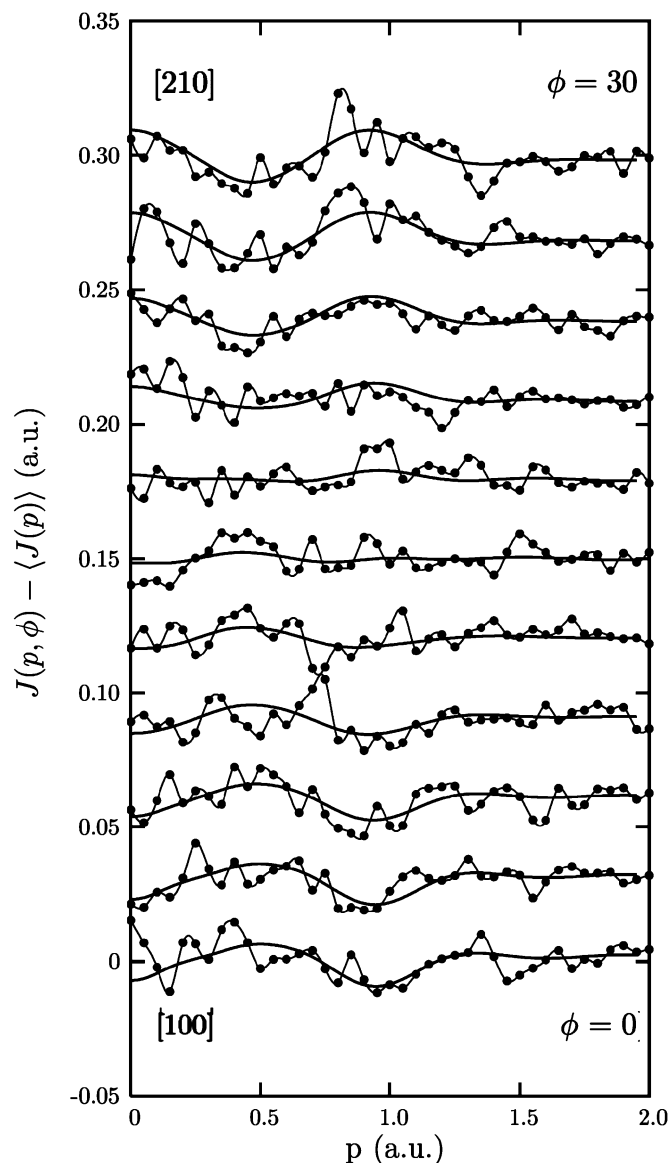
HF level of approximation is reduced when the instantaneous electron correlation is taken into account, but only to a minor extent (see inset). A similar effect, but more important, has been shown to occur in urea[14] and silicon.[15,16]

In order to attempt an explanation of the EMD anisotropy features, let us now take into consideration the characteristics of the WFs and their participation in the EMD.

Table I reports some characteristic parameters of the four symmetry-independent WFs of the reference cell, as obtained from the use of the four one-electron Hamiltonians X here considered. They are centered close to one of the six equivalent oxygen atoms (O^1) in the primitive cell. W_1 and W_2 lie along the bonds between O^1 and its two Si neighbors, which are at a distance from O^1 of 1.613 and 1.605 Å, respectively; W_3 and W_4 can be identified with the two lone pairs of O^1.
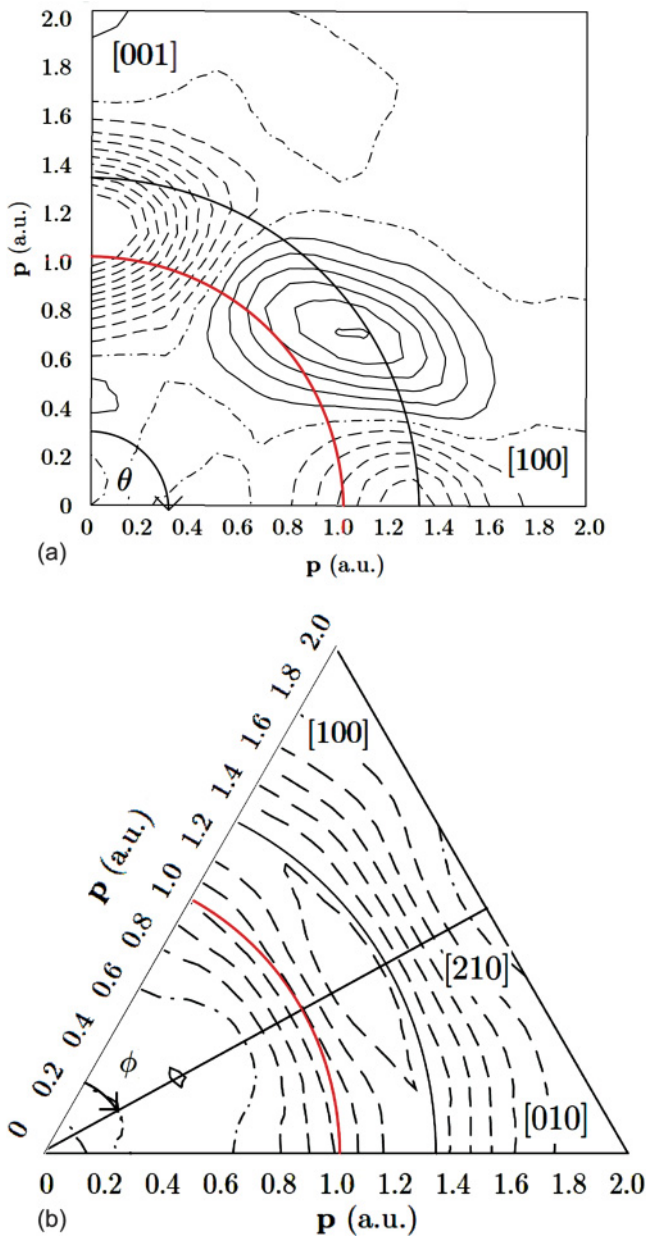
FIG. 5. (Color online) Anisotropy map of the EMD of α-quartz as computed at HF level: (a) in a vertical plane; the vertical ($\theta = 0°$) and horizontal ($\theta = 90°$) axes coincide with the [001] and [100] crystallographic directions, respectively; (b) in the horizontal plane; the directions represented by $\phi = 0°$ and $\phi = 30°$ coincide with the [100] and [210], respectively. The step between isolines is 0.01 a.u. and the maximum and minimum values reported are 0.1 and -0.1 a.u. in both panels. The red thick and the black thin lines mark the region of the map where $|\mathbf{p}| = 1.0$ and 1.3 a.u., respectively.

$R_i = [\int d\mathbf{r} W_i(\mathbf{r})^2(\mathbf{r} - \mathbf{C}_i)^2]^{1/2}$ is a measure of the spread of the ith WF about its centroid $\mathbf{C}_i$. The localized nature of the WFs can be appreciated from these results. It is seen that the HF WFs are more localized than the DFT ones; as usual, the B3LYP result is intermediate between the two. It is also seen that the lone-pair WFs are more diffuse than the bond ones. δ_i is the distance of $\mathbf{C}_i$ from the reference O^1 atom; for all WFs and Hamiltonians these values are very small,
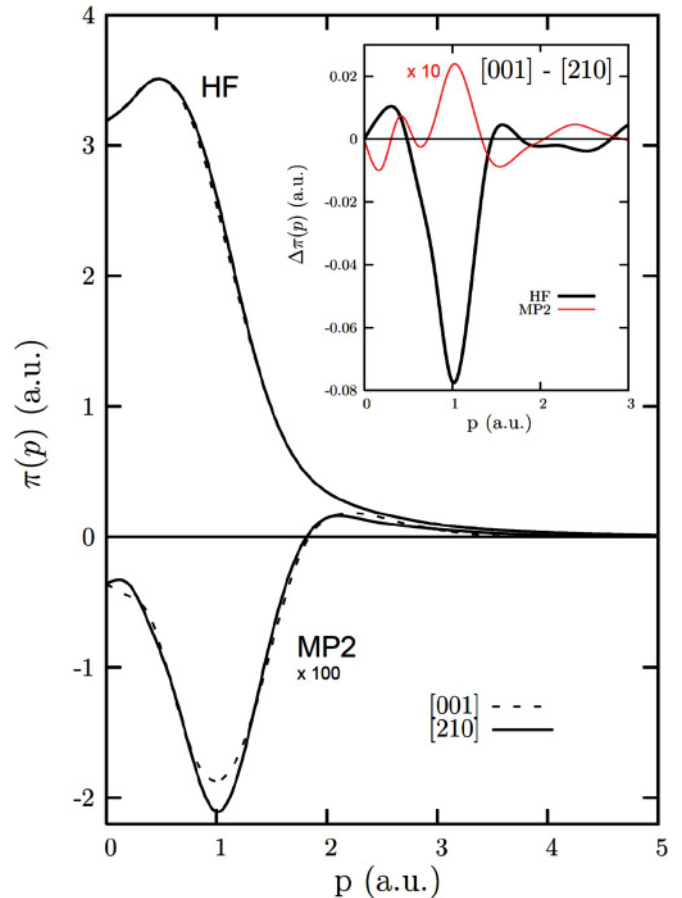

FIG. 6. (Color online) The HF EMD [$\pi^{HF}(\mathbf{p})$] and the MP2 correction to it [$\pi^{MP2}(\mathbf{p})$] plotted along two orthogonal directions, [001] and [210]. The inset reports the difference between the two directions [$\Delta\pi^{HF}(\mathbf{p})$, $\Delta\pi^{MP2}(\mathbf{p})$] in an expanded scale. Note that the MP2 data are multiplied by factors of 100 and 10 in the main plot and in the inset, respectively.

more so for HF than for DFT. This is an indication of the ionic character of α-quartz; as expected, the two WFs along the O–Si bonds are somewhat farther apart with respect to the two lone-pair WFs. The ionic character is confirmed by Q_i, the value of the contribution of O^1 to W_i obtained from a Mulliken-type population analysis: a value $Q_i = 1$ would mean that only GTOs centered in O^1 contribute to W_i. Again, the ionic character is higher for the lone-pair than for the bond-type WFs and, in each category, more so for the HF than for the DFT values. The latter result can explain why HF anisotropies of CPs are less pronounced than DFT ones. Finally, $\overline{f}_i^X = \langle W_i^X | \hat{f}^X | W_i^X \rangle$ is the expectation value of the Hamiltonian with reference to the top of the valence bands. It is seen that the two bond WFs (W_1 and W_2) are considerably lower in energy, as expected, than the two lone-pair ones (W_3 and W_4). The HF values are lower than the DFT ones, while the B3LYP results are intermediate. The four Hamiltonians provide $\overline{f}_i^X$ values rather similar to each other (within $\approx$30%), while the corresponding main gaps may differ by almost a factor of 3 (624, 220, 227, and 305 mhartrees for HF, LDA, PBE, and B3LYP, respectively).

TABLE I. Characteristic parameters of the four symmetry-independent Wannier functions W_i of α-quartz associated with the reference oxygen (O^1), as obtained from the use of the various one-electron Hamiltonians (see text for details).

i (type)	X	R_i^X (Å)	δ_i^X (Å)	Q_i^X ($|e|$)	$\overline{f}_i^X$ (mhartrees)
	HF	1.369	0.404	0.853	-402
1 (long bond)	LDA	1.423	0.415	0.806	-329
	PBE	1.416	0.412	0.813	-331
	B3LYP	1.399	0.410	0.825	-346
	HF	1.368	0.402	0.843	-410
2 (short bond)	LDA	1.467	0.390	0.817	-304
	PBE	1.438	0.391	0.822	-307
	B3LYP	1.413	0.394	0.830	-330
	HF	1.445	0.283	0.949	-230
3 (lone pair 1)	LDA	1.531	0.270	0.912	-167
	PBE	1.515	0.269	0.920	-171
	B3LYP	1.493	0.273	0.927	-181
	HF	1.467	0.286	0.928	-224
4 (lone pair 2)	LDA	1.556	0.315	0.857	-188
	PBE	1.543	0.311	0.865	-187
	B3LYP	1.524	0.303	0.880	-231

Information about the EMD partition among WFs is provided by the 3×3 "i-projected kinetic energy matrix" $\mathbf{T}^{(i)}$, with elements $T_{mn}^{(i)} = (1/2) \int d\mathbf{p}\, \pi_i(\mathbf{p})\, p_m p_n$. Its trace gives the contribution of the ith WF to the kinetic energy, while its eigenvalues, reported in Table II, describe the asymmetry of that WF in momentum space. The present data confirm the similarity of the two bond WFs and of the two lone-pair ones; the kinetic energy of the former is considerably larger than that of the latter. For all WFs it is seen that one of the eigenvalues, marked as τ_a in Table II, is larger than the other two (τ_b and $\tau_{b'}$) by about 20%–30%. The analysis of the corresponding eigenvectors shows that the long axis is oriented almost exactly along the direction which joins the centroid of the WF to the respective oxygen atom: $\mathbf{e}_a^{(i)} \approx (\mathbf{C}_i - \mathbf{R}_{O^1})/|\mathbf{C}_i - \mathbf{R}_{O^1}|$.

This result is still another example of the nonvalidity of the *bond-directional principle*,[5] which predicts that the second momentum of a bond function in $\mathbf{p}$ space is smallest in the bond direction (see Introduction). In order to explain why the reverse is true here, we have plotted in Fig. 7 a map of $\pi_1(\mathbf{p})$ in the Si–O^1–Si plane in two orientations. It is seen that $\pi_1(\mathbf{p})$ exhibits two peaks along the direction of the (long) O^1–Si bond with

TABLE II. Directionality in momentum space of the four reference WF EMDs $\pi_i^{HF}(\mathbf{p})$ and of their sum $\pi_{(O)}^{HF}(\mathbf{p})$, as defined by the eigenvalues of the matrix $\mathbf{T}^{(i)}$. The expectation value of the kinetic energy is reported in the last column. All values in a.u. See text for details.

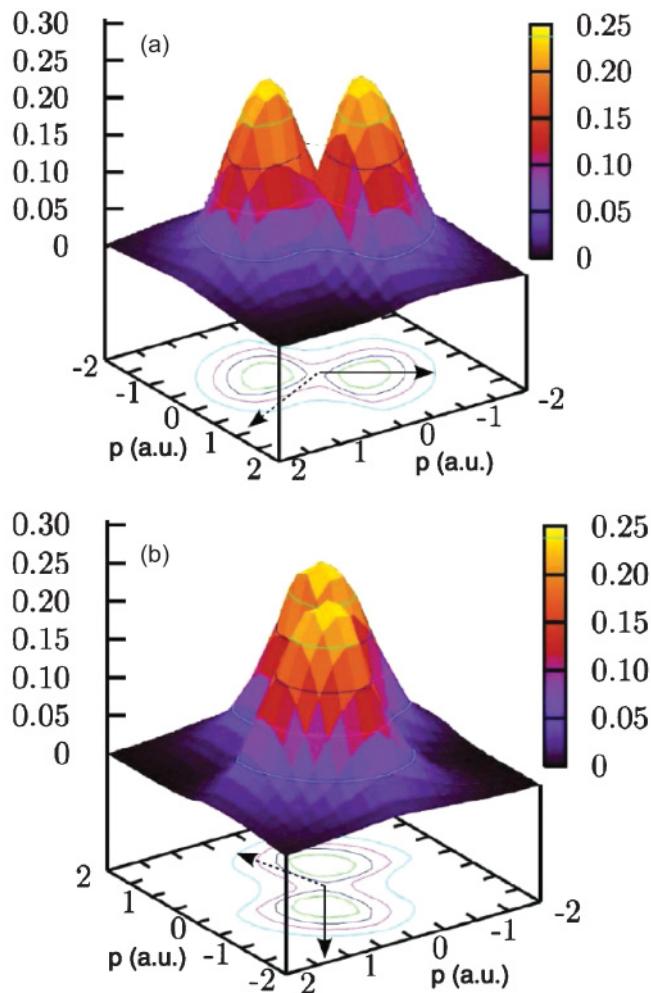| i (type)	τ_a	τ_b	$\tau_{b'}$	$\langle i|\hat{T}|i\rangle$
1 (long bond)	2.302	1.911	1.890	6.103
2 (short bond)	2.371	1.919	1.903	6.193
3 (lone pair 1)	1.613	1.182	1.159	3.955
4 (lone pair 2)	1.509	1.162	1.154	3.826
O (all four WFs)	6.613	6.743	6.742	20.069

FIG. 7. (Color online) Plots of the contribution to the total EMD by a bond WF [$\pi_1(\mathbf{p})$] in atomic units. The plots are referred to $\mathbf{p}$ values in the Si–O^1–Si plane, and are drawn in two different perspectives, parallel or perpendicular to the long Si–O^1 bond along which W_1 is centered: the corresponding direction and that of the short bond are indicated by a continuous and a dotted arrow, respectively. The distance between isolines is 0.05 a.u.

maxima at $|\mathbf{p}| \approx 1.1$ a.u.; it is therefore clear that the second momentum of the distribution in that direction (τ_a) is larger than that in the two orthogonal directions ($\tau_b \approx \tau_{b'}$): $\pi_1(\mathbf{p})$ has in fact quasicylindrical symmetry about the bond. This two-peak structure is typical of bonds with large participation of p AOs, as is here the case.[7] The *new bond-directional principle*[9] (a reformulation of the previous one, proposed by Tanner some years later) appears, however, to be satisfied in the present case (compare the steepness of the peaks in the two directions in Fig. 7). We quote from Ref. 9: "In a chemical bond $\cdots$ there are values $\mathbf{p}_m \cdots$ which correspond to local maxima of $\pi(\mathbf{p}) \cdots$ determined by both the geometric and electronic symmetries of the molecule. For momenta $\mathbf{p}_m + \delta\mathbf{p}$ near a maximum it is more likely that $\delta\mathbf{p}$ is perpendicular rather than parallel to the bond axis."

A similar structure is present in all four WFs, as it is also apparent in Table II from the respective anisotropies.
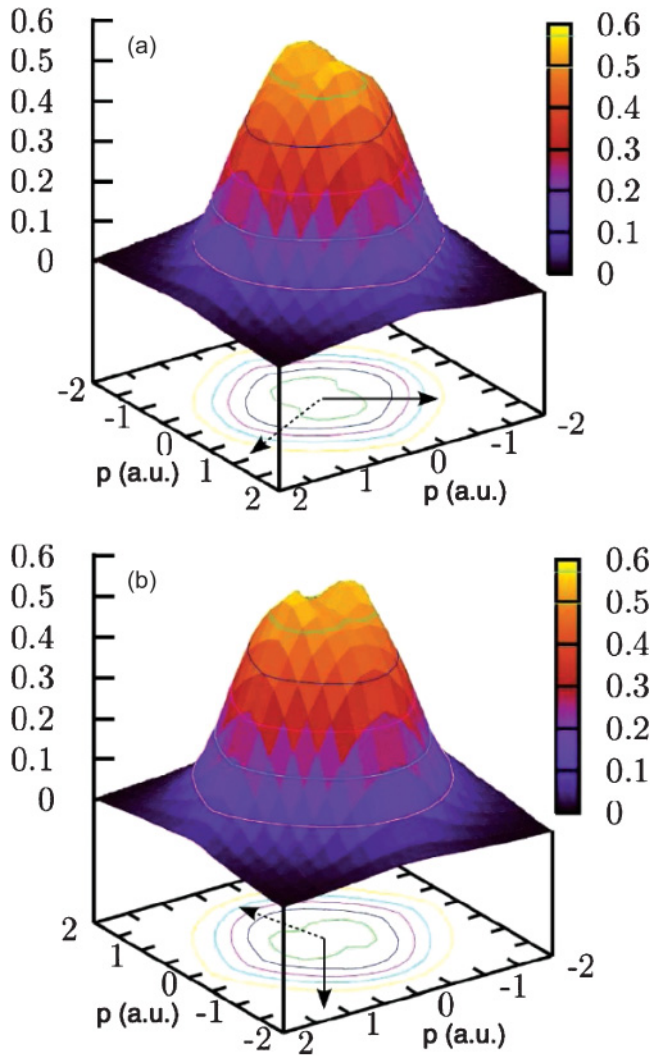
FIG. 8. (Color online) Plots of the contribution to the total EMD by the set of the four WFs at the reference oxygen O^1 $[\pi_{O1}(\mathbf{p})]$ in atomic units. The distance between isolines is 0.1 a.u. Other settings as in Fig. 7.
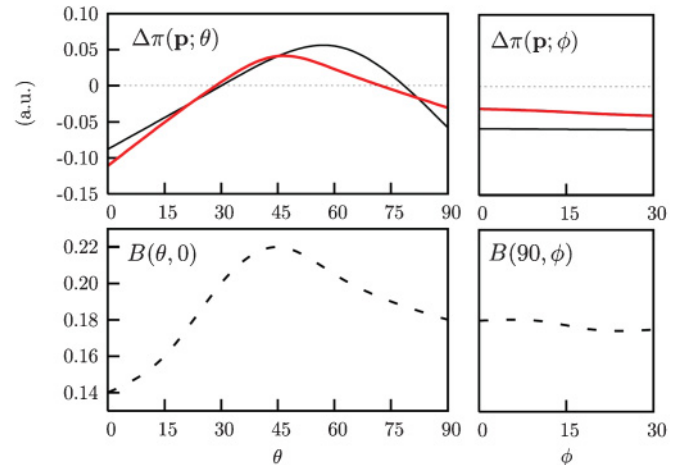

FIG. 9. (Color online) Upper panels: EMD anisotropy $\Delta\pi(\mathbf{p})$ on the vertical (left) and horizontal (right) planes of Fig. 5 for $|\mathbf{p}| = 1.0$ a.u. (red thick continuous line) and $|\mathbf{p}| = 1.3$ a.u. (black thin continuous line). Lower panels: Dimensionless orientation index B_O (see text for the definition) in the two planes. All the quantities of left and right panels are reported as functions of the angles θ and ϕ, respectively.

The sum of the four WF EMDs associated with the reference O^1 oxygen, $\pi_{O1}(\mathbf{p}) = \sum_{i=1}^{4} \pi_i(\mathbf{p})$, provides a partition of the EMD among six symmetry-equivalent substructures in the unit cell. Diagonalization of the corresponding O-projected kinetic energy $\mathbf{T}^{(O)}$ results in the data reported in the last line in Table II. It is seen that the anisotropy is considerably reduced with respect to that of the individual WFs. We still have a quasicylindrical structure, which, however, is now rather flat than oblong; furthermore, the difference between the small and the two larger eigenvalues is here only 2%, namely, an order of magnitude lower. The same type of structure is apparent from the plot of $\pi_{O1}(\mathbf{p})$, reported in Fig. 8.

This is an example of the *compensation principle* formulated in the Introduction, according to which anisotropies in $\mathbf{p}$ space associated with individual substructures are strongly reduced when the respective contributions are summed together. Its explanation is clear in the present case. Each of the four WFs centered about an oxygen atom describes a pair of electrons in a spatially oriented orbital. On the whole,

however, they must reproduce the EMD of an oxygen ion (which is spherical by necessity), only slightly distorted by the crystalline environment. A similar effect, although to a lesser extent, can be expected in the case of covalently bonded atoms.

Yet some trace of EMD anisotropy about each oxygen atom is seen to be left, and the partition into WF contributions has allowed us to describe it qualitatively: as is seen from Fig. 8, $\pi_{O1}(\mathbf{p})$ is approximately cylindrical, with the cylinder axis oriented along $\mathbf{e}_1^{bi}$, the bisector of the Si–O^1–Si angle. We want to show how this feature is reflected in the EMD anisotropy of α-quartz. Consider a set of (quasi)cylindrical objects ω_m ($m = 1,n$) each characterized by a unit vector $\mathbf{e}_m$ directed parallel to the cylinder axis and by an asphericity factor α_m, which is positive or negative according to whether the object is oblong or flat. For each given direction identified by the unit vector $\mathbf{e}(\theta,\phi)$ we can then introduce an *orientation index* of the set: $B(\theta,\phi) = \sum_m \alpha_m |\mathbf{e}_m \cdot \mathbf{e}(\theta,\phi)|/n$.

If all objects have the same asphericity factor α, the orientation index may vary from 0 to α, the two extremes occurring when all objects are directed perpendicular or parallel to $\mathbf{e}(\theta,\phi)$. We apply here the above definition to the set of the six equivalent oxygen atoms in the unit cell, with a direction specified by their special axis in $\mathbf{p}$ space, $\mathbf{e}_m^{bi}$, all characterized by the same α factor, arbitrarily set to 1. Figure 9 reports this orientation index $B_O(\theta,\phi)$ in the vertical plane ($\phi = 0°$, left panel) and in the horizontal plane ($\theta = 90°$, right panel), and compares it with the EMD anisotropy for the two values of $|\mathbf{p}|$ which encompass the region of maximum EMD anisotropy. The correspondence is impressive.

V. CONCLUSIONS

A rich set of directional CPs of α-quartz has been collected along 30 inequivalent crystallographic directions using synchrotron radiation, high-energy x rays at SPring-

8 in Japan. The comparison between the outcomes of the experiment and of *ab initio* simulations has allowed us to discuss the deficiencies of the DFT in describing momentum-space properties and to trace them back to its systematic underestimation of the kinetic energy (i.e., to its failure in satisfying the virial theorem). The agreement is much nicer with HF and post-HF results.

Even if very small, the anisotropy of the EMD has been definitely confirmed by the present experiments; in particular, the vertical plane (containing the [001] direction) has been found to be more anisotropic than the horizontal one (perpendicular to [001]) by about a factor of 2.

A partitioning technique of the EMD of crystalline non-conducting systems, based on the localization of the occupied manifold into Wannier functions, has been presented for the analysis of the contributions to the total EMD coming from different chemical substructures of the crystal; its application to the present case has allowed us to clarify the relationship between the observed EMD anisotropy and the bonding structure of α-quartz.

On the grounds of such a partition scheme, a compensation principle has been enunciated which states that the total EMD anisotropy of a many-electron system is much less than that of the individual chemical substructures (bonds, lone pairs, etc.).

Comparison with other members of the silica family (β-quartz, zeolites, etc.) could provide insight into the transferability of EMD features associated with well-defined substructures.

There is room for improvement both experimentally (counting statistics and set of directions explored) and theoretically (approximate account of nuclear motion effects, inclusion of orbital relaxation in the MP2 correction of the HF density matrix,[41] treatment of the correlation of core electrons).

[1] C. A. Coulson, Proc. Cambridge Philos. Soc. **37**, 55 (1941).

[2] C. A. Coulson, Proc. Cambridge Philos. Soc. **37**, 74 (1941).

[3] P. J. Becker, J. M. Gillet, P. Cortona, and S. Ragot, Theor. Chem. Acc. **105**, 284 (2001).

[4] I. R. Epstein and W. N. Lipscomb, J. Chem. Phys. **53**, 4418 (1970).

[5] I. R. Epstein and A. C. Tanner, in *Compton Scattering*, edited by B. G. Williams (McGraw-Hill, New York, 1977), p. 209.

[6] B. I. Ramirez, J. Phys. B **15**, 4339 (1982).

[7] A. Rozendaal and E. J. Baerends, Chem. Phys. **95**, 57 (1985).

[8] D. L. Cooper and N. L. Allan, J. Chem. Soc., Faraday Trans. 2 **83**, 449 (1987).

[9] A. C. Tanner, Chem. Phys. **123**, 241 (1988).

[10] J. Wang, B. J. Clark, H. Schmider, and V. H. Smith, Can. J. Chem. **74**, 1187 (1996).

[11] K. T. Leung and C. E. Brion, Chem. Phys. **82**, 87 (1983).

[12] K. T. Leung and C. E. Brion, J. Am. Chem. Soc. **106**, 5859 (1984).

[13] C. Edmiston and K. Ruedenberg, Rev. Mod. Phys. **35**, 457 (1963).

[14] A. Erba, C. Pisani, S. Casassa, L. Maschio, M. Schütz, and D. Usvyat, Phys. Rev. B **81**, 165108 (2010).

[15] A. Erba, M. Itou, Y. Sakurai, R. Yamaki, M. Ito, S. Casassa, L. Maschio, A. Terentjevs, and C. Pisani, Phys. Rev. B **83**, 125208 (2011).

[16] C. Pisani, M. Itou, Y. Sakurai, R. Yamaki, M. Ito, A. Erba, and L. Maschio, PhysChemChemPhys **13**, 933 (2011).

[17] M. Rosenberg, F. Martino, W. A. Reed, and P. Eisenberger, Phys. Rev. B **18**, 844 (1978).

[18] D. P. Mahapatra and H. C. Padhi, J. Phys. C **17**, 5517 (1984).

[19] R. Dovesi *et al.*, CRYSTAL09 *User's Manual* (Università di Torino, Torino, 2010) [http://www.crystal.unito.it].

[20] R. Dovesi, R. Orlando, B. Civalleri, C. Roetti, V. R. Saunders, and C. M. Zicovich-Wilson, Z. Kristallogr. **220**, 571 (2005).

[21] A. Erba and M. Halo, CRYSCOR09 *User's Manual* (Università di Torino, Torino, 2010), [http://www.cryscor.unito.it].

[22] L. Maschio, D. Usvyat, F. Manby, S. Casassa, C. Pisani, and M. Schütz, Phys. Rev. B **76**, 075101 (2007).

[23] D. Usvyat, L. Maschio, F. Manby, S. Casassa, M. Schütz, and C. Pisani, Phys. Rev. B **76**, 075102 (2007).

[24] C. Pisani, L. Maschio, S. Casassa, M. Halo, M. Schütz, and D. Usvyat, J. Comput. Chem. **29**, 2113 (2008).

[25] M. Schütz, D. Usvyat, M. Lorenz, C. Pisani, L. Maschio, S. Casassa, and M. Halo, in *Accurate Condensed Phase Quantum Chemistry*, edited by F. R. Manby (CRC Press, Boca Raton, FL, 2010), p. 29.

[26] G. H. Wannier, Phys. Rev. **52**, 191 (1937).

[27] C. M. Zicovich-Wilson, R. Dovesi, and V. R. Saunders, J. Chem. Phys. **115**, 9708 (2001).

[28] S. Casassa, C. M. Zicovich-Wilson, and C. Pisani, Theor. Chem. Acc. **116**, 726 (2006).

[29] P. Pulay, Chem. Phys. Lett. **100**, 151 (1983).

[30] C. M. Zicovich-Wilson and A. Erba, Theor. Chem. Acc. **126**, 165 (2010).

[31] M. Itou and Y. Sakurai, in *Synchroton Radiation Instrumentation*, edited by T. Warwick, J. Stöhr, H. A. Padmore, and J. Arthur, AIP Conf. Proc. No. 705 (AIP, Woodbury, NY, 2004), p. 901.

[32] Y. Sakurai and M. Itou, J. Phys. Chem. Solids **65**, 2061 (2004).

[33] N. Sakai, J. Phys. Soc. Jpn. **56**, 2477 (1987).

[34] F. Biggs, L. B. Mendelsohn, and J. B. Mann, At. Data Nucl. Data Tables **16**, 201 (1975).

[35] C. Pisani, R. Dovesi, and C. Roetti, *Hartree-Fock Ab Initio Treatment of Crystalline Solids*, Lecture Notes in Chemistry Vol. 48 (Springer-Verlag, Berlin, 1988).

[36] A. Erba and C. Pisani, J. Comput. Chem. (in press).

[37] S. Ragot, J. Chem. Phys. **125**, 014106 (2006).

[38] A. J. Thakkar, in *Theory and Applications of Computational Chemistry: The First 40 Years*, edited by C. E. Dykstra, G. Frenking, K. S. Kim, and G. E. Scuseria (Elsevier, Amsterdam, 2005), p. 11.

[39] J. R. Hart and A. J. Thakkar, Int. J. Quantum Chem. **102**, 673 (2005).

[40] R. R. Zope, Phys. Rev. A **62**, 064501 (2000).

[41] D. Usvyat and M. Schütz, J. Phys.: Conf. Series **117**, 012027 (2008).

[42] W. Neutsch, J. Comput. Phys. **51**, 313 (1983).

[43] C. M. Zicovich-Wilson, F. Pascale, C. Roetti, V. R. Saunders, R. Orlando, and R. Dovesi, J. Comput. Chem. **25**, 1873 (2004).

[44] J. P. Perdew and A. Zunger, Phys. Rev. B **23**, 5048 (1981).

[45] J. P. Perdew, K. Burke, and M. Ernzerhof, Phys. Rev. Lett. **77**, 3865 (1996).

[46] A. D. Becke, J. Chem. Phys. **98**, 5648 (1993).

[47] K. Kihara, Eur. J. Mineral **2**, 63 (1990).

[48] P. Pulay and S. Saebø, Theor. Chim. Acta **69**, 357 (1986).

[49] L. Maschio and D. Usvyat, Phys. Rev. B **78**, 073102 (2008).

[50] A. J. Thakkar, Adv. Chem. Phys. **128**, 303 (2004).

[51] Y. Tanaka, Y. Sakurai, A. T. Stewart, N. Shiotani, P. E. Mijnarends, S. Kaprzyk, and A. Bansil, Phys. Rev. B **63**, 045120 (2001).